

Energy-Aware Aggregation of Input Data for the Optimisation of Heat Supply of Municipal Districts

Patrik Schönfeldt ¹ and Elif Turhan ¹

¹German Aerospace Center (DLR), Institute of Networked Energy
Systems, Oldenburg, Germany

December 9, 2025

Abstract

In the context of municipal heat planning, it is imperative to consider the numerous buildings, numbering in the hundreds or thousands, that are involved. This poses particular challenges for model-based energy system optimization, as the number of variables increases with the number of buildings under consideration. In the worst case, the computational complexity of the models experiences an exponential increase with the number of variables. Furthermore, within the context of heat transition, it is often necessary to map extended periods of time (i.e., the service life of systems) with high resolution (particularly in the case of load peaks that occur at the onset of the day). In response to these challenges, the aggregation of input data is a common practice. In general, building blocks or other geographical and urban formations, such as neighbourhoods, are combined. This article explores the potential of incorporating energy performance indicators into the grouping of buildings. The case study utilizes authentic data from the Neu-Schwachhausen district, grouped based on geographical location, building geometry, and energy performance indicators. The selection of energy indicators includes the annual heat consumption as well as the potential for solar energy generation. To this end, a methodology is hereby presented that considers not only the anticipated annual energy quantity, but also its progression over time. We present a full workflow from geodata to a set of techno-socio-economically Pareto-optimal heat supply options. Our findings suggest that it is beneficial to find a balance between geographical position and energy properties when grouping buildings for the use in energy system models.

1 Introduction

In Germany, the heating sector accounts for more than 84 % of the final energy consumption of the residential sector and contributes about a third of the country’s GHG emissions [1]. To guide the necessary process of decarbonisation, the heat planning act (“Wärmeplanungsgesetz”) requires every municipality to submit a heat plan [2]. This type of heat planning needs to consider hundreds to thousands of buildings. In particular for model based optimisation, this imposes a challenges, as worst case the computational time can increase exponentially with the number of variables [3]. Even worse, in the context of heat planning, both long (component lifetimes) and short (peak loads, fluctuations of renewable generation) time scales are important. To face these challenges, aggregation of data is required. On the geographical scale, often building blocks, neighbourhoods, or other groups are introduced by city planers [4, 5]. Secondly, there are building typologies focusing solely on energy [6, 7]. These typically focus on the building demand, independent from potential characteristics of the building stock in a specific area (with exception for localized classification, e.g. [8]) or generation potential. When it comes to generation potential, some works investigate the potential solar gains depending on building types in a neighbourhood [9, 10]. This approach, however, is more linked to a green field approach.

Several years ago, data acquisition could be considered the main issue to elaborate heat transition plans for municipalities. At that time, “common data-driven models apply statistical and artificial intelligence (AI) simulation mainly based on machine learning (ML) methods to model energy use” [11]. With the aforementioned law in action, municipalities are now mandated to collect data for the creation of the heat plans. Additionally, solar maps [12] nowadays are widely implemented. Thus, the focus shifts to availability of planning capacities and on data processing, facilitating a more data-centred approach. From a general perspective, the idea described in this contribution can be described as follows:

1. compress the input data (cf. Sec. 3),
2. process the compressed data (cf. Sec. 4),
3. decompress result data to have result for original dataset (cf. Sec. 5).

If compression and processing the data are commutable, the final result will be the same as if the result of the original data was compressed. Although we are dealing with linear energy system models, even a linear compression method will only fulfil this requirement in edge cases where the energy system model does not reach any constraint.

In the following, we walk through the method using the area of Bremen Neu-Schwachhausen and the corresponding energy geodata as an example. Where meaningful to evaluate the method, we applied simplifying assumptions.

2 Characterisation of input data

2.1 Heat demand

A map showing the annual heat demand of the individual buildings is displayed in Fig. 1. By the bare eye, it is visible that there are darker (less heat de-

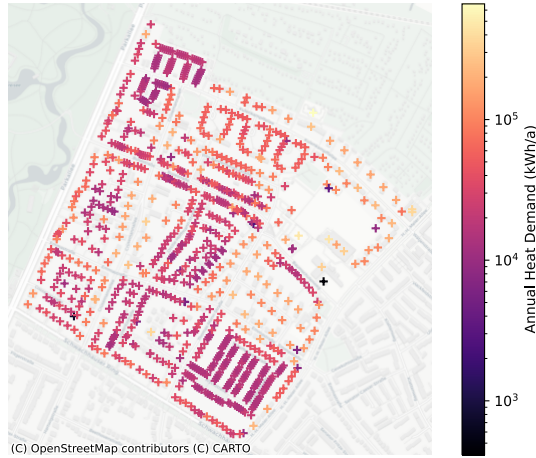


Figure 1: Annual heat demand of all 859 buildings in the area.

mand) and lighter (higher heat demand) areas. This mostly reflects areas with bigger and smaller building sizes and not the achieved building standard. The influence of the building footprint is also dominating the distribution of the annual heat demand as is displayed in Fig. 2. The curve for the absolute heat

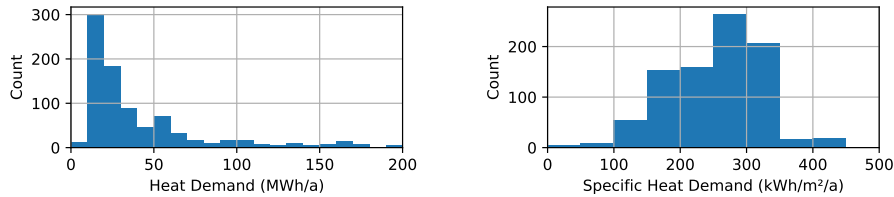


Figure 2: Histograms of the annual heat demand of the buildings in absolute numbers per building (left) and relative to the building footprint (right).

demand peaks before 20 MWh/a, then falls quickly with a long tail starting at 70 MWh/a, which continues to show non-zero values even beyond the scale. The complementary numbers relative to the building footprint can be seen in the right panel of the same figure. This distribution is very compact, outliers are rare, the middle four of the the equally sized bins are all populated by between 150 and 250 buildings.

2.2 Solar potential

When it comes to local energy generation, solar potential marks a key parameter. It can be calculated from roof parameters, that are available, e.g. from LOD2 open data [13]. For this study, we use data from the solar map of Bremen, that also includes shadowing by trees. As buildings in urban areas are aligned with streets, which follow an almost orthogonal pattern in the region we investigate, the roof azimuth groups in four different orientations. As displayed in Fig. 3,

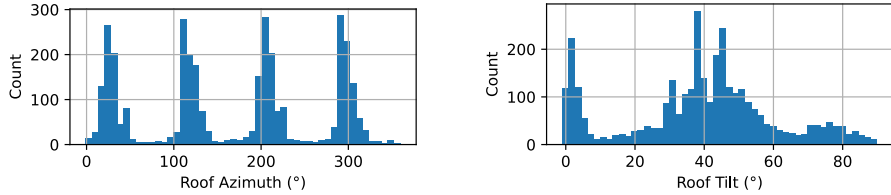


Figure 3: Histograms of the roof azimuth (left) and roof tilt (right).

these corresponding groups are rather distinct. However, it has to be kept in mind that later not the individual roofs but the buildings they cover are important. The roof tilt follows a not so clear distribution, an interpretation might need to include knowledge about the psychology of architects.

However, what we are actually interested in is not the shape of the building but its energy-related properties. Thus, we apply a method to our knowledge first described in [14]. The idea is to approximate the generation potential curve of every roof by a linear combination of the generation potential curves of N ‘standard roofs’

$$P_{\alpha,\theta}(t) \approx \sum_{n=0}^{N-1} w_n \times P_n(t). \quad (1)$$

This way, there is a distinct quantity (the weight w_n of the ‘standard roof’) that clustering can use. When compared to using the annual solar potential instead, this new method preserves information about the temporal structure on a finer temporal resolution. Later, the factors w_n can be used with the solar potential time series P_n to reproduce the solar potential time series for every building. It should be mentioned that it is still an ad-hoc model, that has been shown plausible but is missing a proper validation according to scientific standards.

While it is possible to find the coefficients w_n e.g. using a least square fit, [14] suggests to just solve a set of linear equations. One argument to do so is the reduction of computational load, which can be important especially for large datasets. When picking a discrete number of times of the day $0 \text{ h} \leq t_d < 24 \text{ h}$ and the same number of representative roofs (defined by a combination of α and θ), the set of equations to solve in order to obtain the w_n is defined by

$$\langle P_{\alpha,\theta} \rangle(t_d) = \sum_{n=0}^{N-1} w_n \times \langle P_n \rangle(t_d) \quad \forall t_d, P_{\alpha,\theta}, P_n \quad (2a)$$

where

$$\langle P_x \rangle(t_d) = \frac{1}{365} \times \sum_{d=0}^{364} P_x(d \times 24 \text{ h} + t_d), \quad (2b)$$

with $P_x \in \{P_{\alpha,\theta}, P_n\}$ is the power at that time of the day averaged over the whole year. (Note that Eq. 2 assumes consistent time throughout the year, i.e. daylight saving time has to be considered manually.) For the present study, the standard roofs are chosen to have a common tilt of $\theta = 30^\circ$ and azimuth angles of $\alpha \in (90^\circ, 180^\circ, 270^\circ)$. Further we choose $t_d \in (9 \text{ h}, 12 \text{ h}, 15 \text{ h})$. Results produced using this method are displayed in Fig. 4.

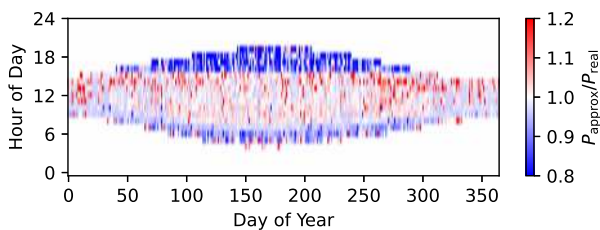


Figure 4: Fraction of approximated over real solar power potential values over the year.

For the present example, the approximation works quite well in the range defined by the chosen t_d . Here, the deviation is typically in the single percent range. However, there is a systematic underestimation of the power in early mornings and late evenings, particularly in summer. As absolute numbers approach low values at these times, we assume an acceptable impact of this bias.

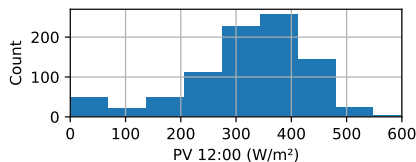


Figure 5: Histogram of the solar energy generation potential (relative to building footprint, not to roof area).

The distribution of a corresponding, derived quantity (PV potential at noon) for all buildings in the area can be seen in Fig. 5. This quantity, again, is more compact compared to the original quantities. In our dataset, we also find four buildings with extraordinary high solar potential relative to the building footprint ($P_{\text{peak}} > 600 \text{ W/m}^2$). These values are outliers but no obvious error, as the roof area can exceed the building footprint because of the roof tilt. As the method we apply later is rather robust against these types of data errors,

we can just accept them. For this particular area, we also observe that there is a strong linear correlation between the solar potential at different times of the day. As this might be due to the high amount of parallel buildings in the dataset (cf. upper histogram in Fig. 3), we do not generalise this finding and use $\langle P_{\alpha,\theta} \rangle(t_d)$ for all of the chosen t_d to describe the solar potential.

2.3 Cost of heat network connection

The cost of heat network connection is per building, but as we work with values relative to the building footprint, we need to treat the costs for heat network connections the same way. We estimate the costs of the heat network connection by first computing the peak heat demand according to a BDEW (‘Bundesverband der Energie- und Wasserwirtschaft’, German for ‘National Association of Energy and Water Industries’) demand profile assuming a single family house [15]

$$\hat{P}_{\text{th}}[\text{kW}] \approx 0.228 \times E[\text{MWh/a}]. \quad (3)$$

This number is then used for a cost estimation of a heat network connection according to the KWW Technikkatalog [16] as

$$C_{\text{HNC}}(\hat{P}_{\text{th}}) = 13.4111 \text{ €/kW} \times \hat{P}_{\text{th}} + 13976 \text{ €}. \quad (4)$$

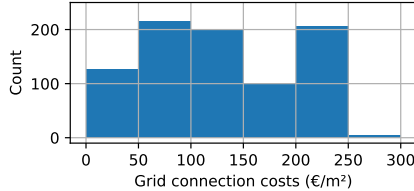


Figure 6: Histogram of the grid connection costs (relative to building footprint).

The distribution is displayed in Fig. 6. There are four outliers, with values above 300 €/m^2 up to close to 600 €/m^2 . That this number equals the number of outliers with very high solar potential, is pure coincidence: These high-cost buildings have a solar potential of 0 kW/m^2 .

3 Vector quantisation

We search for buildings that are similar, i.e. that can meaningfully rely on the same heating solutions. The similarity includes two aspects: location and energy. Because clusters exist in n -dimensional data space, they often overlap in their projection to a two-dimensional plane. When focusing on decentralised heat supply options as in [14], this is no issue. However, it would be a bad assumption that supply using a new heating grid is equally suitable for every

single building in a geographically scattered cluster. In fact, we identify different requirements for the clustering algorithm for energy and spatial indicators: Energy-wise, clusters should be as homogenous as possible to be able to propose the same building energy system for all of them. Location-wise, the extent of the clusters might not be as crucial as long as the area is connected, i.e. suitable for a common centralised solution. For all the methods, the data has been normalised to the range [0:1] using the `MinMaxScaler` of [17].

3.1 Data-based building categories

As a first step, we cluster based on energy values. The goal is to automatically derive building categories tailored to both the data and the optimisation process. Because we want every building within one cluster to be represented by one representative building, clusters should be compact in the sense that the standard deviation within the cluster should be low for every value. This property is served by K-Means clustering. As a side-note, clustering including integer dimensions is also possible when K-Medoids [18] is used instead of K-Means. This might be required, e.g. if the model included a discrete number of inhabitants as a variable.

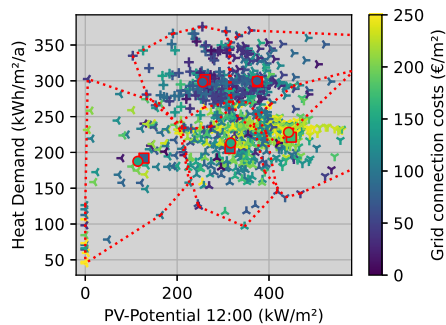


Figure 7: Scatter-plot of all buildings with respective footprint-specific energetic quantities. Five clusters are identified using different markers and grouped by lines. Possible cluster representatives are drawn as disks (average values per building, original K-Means centres) and as squares (building values weights by building footprint).

For the current case study, however, the considered values are positive real numbers. We have specific heat demand in $\text{kWh/m}^2/\text{a}$, solar potential in the morning (9 am), at noon (12 pm), and in the afternoon (3pm), all in W/m^2 , and costs for a heat grid connection in €/m^2 , where the m^2 reflects the building footprint for all five quantities.

The result of an example clustering (five clusters) using all of the aforementioned energetic properties is displayed in Fig. 7. Note that the clusters overlap only in the 2D projection. There are two high-demand clusters, that both also

Method	Variables		Network Length (m)	
	min	max	min	max
K-Means	25	378	30.8	31.9
K-Means Energy	19	187	41.6	64.5
K-Prototypes	23	197	40.0	88.1
K-Prototypes after HDBSCAN	20	193	39.4	80.9
K-Modes	8	67	50.2	119.3

Table 1: Extreme values in the 2-step clustering scan

feature relatively low grid connection costs, one with medium and one with high solar potential. These are complemented by three low-demand clusters with higher grid connection costs, one of those also features low solar potential. That the cluster centre of the values relative to the building footprint is very close to the building footprint-weighted average corresponds to the fact that for this particular dataset

$$\sum_{b \in \mathfrak{B}} A_b \times \sum_{b \in \mathfrak{B}} \frac{x_b}{A_b} \approx N_b \times \sum_{b \in \mathfrak{B}} x_b, \quad (5)$$

where \mathfrak{B} is the set of building indexes, x_b is any quantity of building b (e.g. its annual heat demand), and A_b is the footprint of that building. This means that in this case the method using representatives expressed in specific quantities does not bias the summed values of the clusters.

3.2 Geographical grouping

In this second step, buildings are grouped considering (also) their geographical locations. These groups will be used to decide on heat-network connections. As connections are not realised in a star topology but using line strips, compactness is not as important as for the building categories, which leaves a rich set of options for potential algorithms, including DBSCAN [19], OPTICS [20], and HDBSCAN [21]. While we do not do this here, note that these also allow for using a custom definition for the distance between two points.

While certain configurations – particularly doing the same thing for all buildings – are possible independent from the grouping, other options depend on the clustering method. We did a scan over different numbers for both, representative buildings and geographical groups. This scan ranged from 5 to 30 for both, representative buildings and geographical groups. Results are summarized in Table 1. A visualisation and deeper discussion of the results can be found in Appendix A. We find that there is a trade-off between the total number of variables needed for the model and the geographical cohesion of the geographical groups. We measure the latter by calculating the average length to connect buildings of only one geographical group to a heat network. In the following, they described further interwoven with the descriptions of the methods.

K-Means Clustering using geographic location. This leads to geographically dense, non-overlapping groups. While the single-group line length is almost constant using this method, increasing the number of representative buildings or the number of geographical groups leads to an almost proportional increase of the number of variables.

K-Means Energy K-Means clustering using geographic location and energy data. These groups are still geographically dense but allow for some overlap to reflect similarities of buildings. In our scan, this approach about halves the number of variables at the cost that the average line length now increases with the number of representative buildings.

K-Modes K-Modes [22], generalises K-Means for categorical data. In a first sub-step, connected areas within buildings of the same building category are identified using HDBSCAN. In a second sub-step, the labels from the HDBSCAN runs and the building categories (from step 1) are used to find the final groups. As this method focuses on finding groups containing as few representative buildings as possible, it clearly reduces the number of variables in the model. This comes at the cost of increased line length if only one geographical group is connected to using heat network.

K-Prototypes This algorithm combines K-Modes with K-Means to handle datasets with mixed scalar and categorical data [22, 23]. This way, building categories and geographical locations can be considered. In the scan, an increase in the number of geographical clusters has a bigger impact on the number of variables compared to an increase of the number of representative buildings. Line length also increases for both but not as much as with K-Modes.

K-Prototypes after HDBSCAN A combination of geographic location, building categories, and labels of HDBSCAN is used. Compared to pure K-Prototypes, this method comes with less increased intra-cluster line length when both energy and final clusters are high. On the other hand, the number of variables increases slightly more with the number of representative buildings (starting from a lower minimum).

As they provide very similar performance, in the following, we drop the application of K-Prototypes without the extra HDBSCAN. An example assignment of the presented two-step methods using five representative buildings and ten geographical groups is shown in Fig. 8. It is visible that the methods have different geographical cohesion. Still, the assignment is also clearly considering the location, as seen in a number of very localised groups (light green, red, grey) even in the K-Modes example.

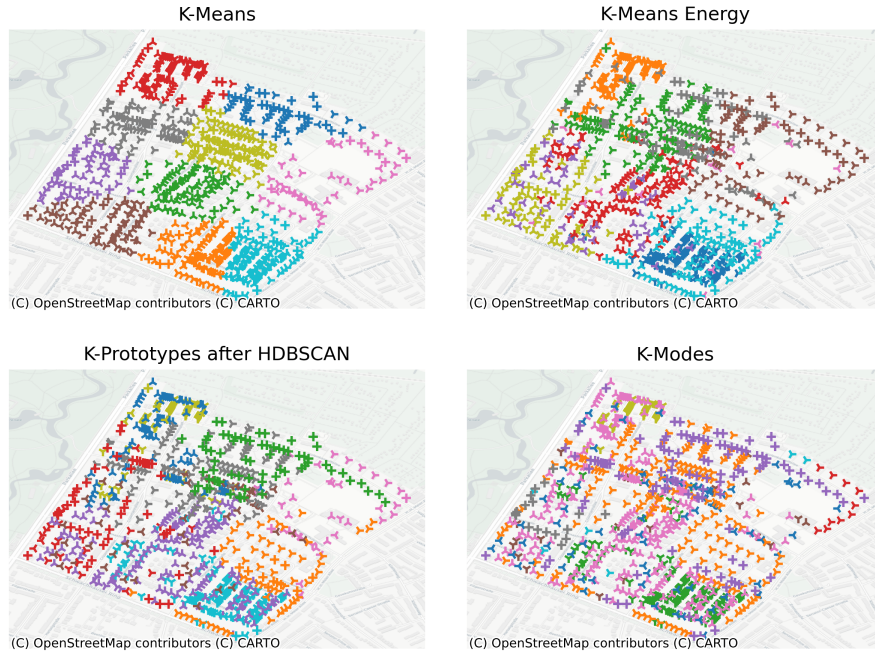


Figure 8: Assignment of buildings to representative buildings (icons) and geographical groups (colours) for the case of five representative buildings and ten geographical groups.

4 Optimisation model

The optimisation is an iterative process performed using a heuristic search. For every archetype building, we investigate the two options of a centralised (i.e. heat network) or a decentralised heat supply. For both of them, the size of the PV system is optimised, for the latter also the choice between installing a new air source heat pump and keeping an (assumed to be existing) gas boiler. If better data about currently existing heating technologies was at hand, it should be considered in the clustering and would translate to price differences for different technologies.

Note that we decided on parameters in a way that the influence of the clustering method can be studied. Thus, technologies should have clear advantages and disadvantages. For example, keeping a gas boiler results in operation costs but no investment costs. Secondly, there is a decision between the centralised and the decentralised option of a building per geographical group. This is where the number of combinations becomes relevant. For the present study with five representative buildings in ten geographical groups, the number of combinations of representative buildings and geographical groups, which is the number of decision variables in the optimisation, as well as the shortest possible heat grid

Method	Variables	Shortest grid
K-Means	50	275m
K-Means Energy	31	26m
K-Prototypes after HDBSCAN	29	83m
K-Modes	12	1754m

Table 2: Number of variables, as well as shortest possible heat grid (one group, one representative building).

when selecting only one of these combinations is shown in Tab. 2.

For the supply of the heat network, we assume a central heat pump that has access to waste heat (COP of 8), while decentralised heat pumps use the ambient air (COP ranging between 2.4 and 6, depending on the season and time of the day). After the decision is made, which buildings are connected, we use a minimum spanning tree [24] to find the length of the heat network. To estimate the power required for groups of buildings using a standard load profile, we apply an empirical formula for the diversity factor of n buildings [25],

$$q_{\text{diversity}}(n) = \min \left(1, a + \frac{b}{1 + (n/c)^d} \right), \quad (6)$$

with $a = 0.450$, $b = 0.551$, $c = 53.8$, and $d = 1.76$ (rounding to three significant digits by us). The formula originally targeted $1 < n \leq 200$, but as it approaches almost constant values afterwards, we also use it for higher numbers of buildings. In particular, by dividing the peak load of the standard load profile in the limit $q_{\text{diversity}}(n \rightarrow \infty) \approx 0.47$, we find the peak load for one building. Note that the formula was derived using data from only two heat networks, so the method has to be understood as a rough approximation. The presented aggregation method works independently from the chosen energy system model for the representative buildings. Thus, we apply a rather simple model which is presented in Appendix B.

Using the number of the occurrences of the representative buildings in the geographical groups $N_{b,g}$, the global indicators can be computed for total energy costs in 2025

$$C_{E,2025} = C_{\text{el,HN}} + \sum_{b \in \mathfrak{B}} \sum_{g \in \mathfrak{G}} N_{b,g} C_{b,g} \quad (7a)$$

with the set of group indexes \mathfrak{G} , the electricity costs for the heat network $C_{\text{el,HN}}$ and the energy costs per building $C_{b,g}$ (see Eq. 13a), and for annualised investment costs

$$C_{\text{invest}} = C_{\text{HN}} + \sum_{b \in \mathfrak{B}} \sum_{g \in \mathfrak{G}} \sum_{i \in \mathfrak{I}} N_{b,g} C_{i,b,g}, \quad (7b)$$

with the set of technologies to be invested in de-centrally \mathfrak{I} , their annualised costs $C_{b,g,i}$. At last, with $P_{\text{el}}(t)$ the electrical and P_{gas} the gas consumption time series if the complete area, the green house gas emissions are calculated as

$$m_{\text{GHG}} = \int \frac{f_{\text{el}}}{4} \max(P_{\text{el}}(t), 0 \text{ kW}) + f_{\text{gas}} P_{\text{gas}}(t) dt, \quad (7c)$$

where $f_{\text{el}} = 260 \text{ g/kWh}$ and $f_{\text{gas}} = 240 \text{ g/kWh}$ are the specific emission factors for 2025 and the factor $1/4$ reflects the assumption that the average emissions will be $1/4$ of that value over the lifetime.

After all indicators are evaluated for the system, the heuristic tries new values for the variables. Details about this method can be found in [26]. (As we decided to not include energy storage in the present study, the operation is inflexible and not optimised here.) For the present study, we allow 100 000 generations in a population of 16 using the Non-dominated Sorting Genetic Algorithm II [27] as available in PyGMO [28]. Leaving more time for the algorithm will increase the likelihood of sampling more of the Pareto-plane. However, we use the quality of the results as an indicator to access the sampling methods.

The result of this method is a set of (nearly) Pareto-optimal configurations for the energy-system. It should be noted that the sampling of the solution space is random. This implies that the density of points does not contain any information. In particular, a) the non-existence of a configuration in the result data does not mean that it is not Pareto-optimal and b) points at the edge of the sampled Pareto-hyperplane might not be the most extreme possible options. We will see a concrete example in the next section.

5 Data analysis

To get an overview over the multitude of Pareto-optimal solutions, it makes sense to also work with aggregated values instead of only looking at every single option for every single representative building in each of the geographical groups. After the general overview, we will look into example configurations resulting from the optimisation. These configurations can be seen as the decompressed results, as they view at every individual building again.

In the present study, heat can be provided by one of the three options, gas boiler, heat pump, and heat network. Fig. 9 shows which area of the possible combinations has been sampled by the Pareto-search. It is clearly visible that one particular Pareto-optimal solution has not been sampled by any of the runs: In our model, not replacing any gas boiler and not installing any PV would have resulted in no investment costs which is trivially Pareto-optimal. However, when looking at the (in this case also three-dimensional) space of conflicting goals, as displayed in Fig. 10, it can be seen that already the found solutions approach rather low investment values.

In the comparison of the four clustering methods, three produce similar aggregated configurations (Fig. 9) as well as similarly shaped Pareto-planes (Fig. 10). From this perspective, K-Modes deviates most, as it has a lower density of sampled points. It does also not find the elbow at the front of only investment and operational costs. At this one-dimensional front, the other methods show a point at about -1000 €/Pers/a of energy costs, where additional investment starts to reduce the energy costs with a reduced slope. One reason for this might be that configurations are made impossible by the reduction of variables (cf. Tab. 2): When the geographical groups strongly align

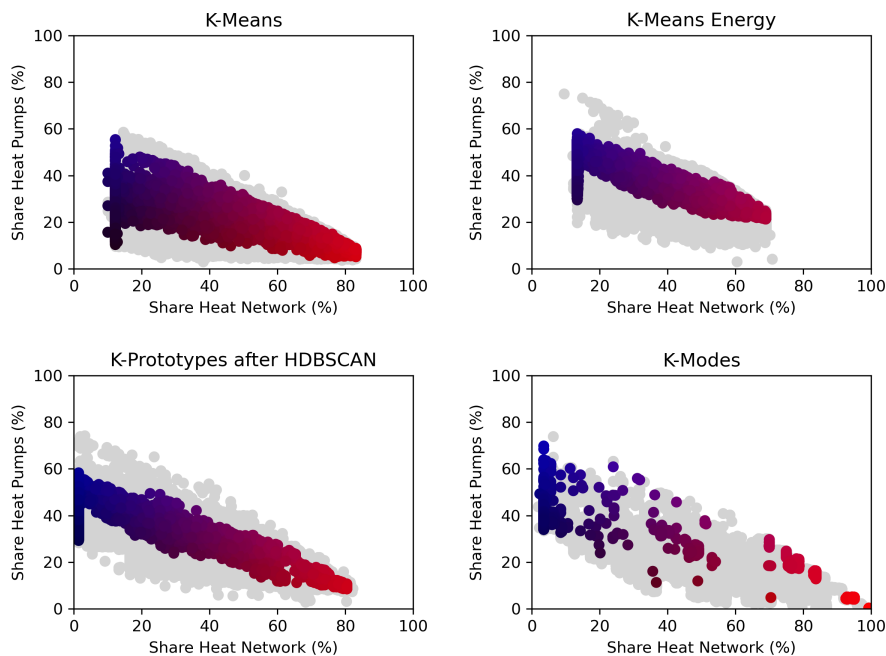


Figure 9: Sampled Pareto-plane in terms of global share of heating technologies for four different aggregation methods. Discarded solutions are displayed in gray, Pareto-optimal solutions are coloured. As the three add up to 100 %, the colour information (black: gas boiler, blue: heat pump, red: heat network) is redundant.

with the presence of specific representative buildings, it is there is decreased possibility to connect a heat network just in direct neighbourhoods. The reason is that neighbouring buildings a different representative building type are often in a different geographical group (cf. Fig 8). For purely geographical K-Means on the other extreme side, neighbouring buildings of the same representative building type are more likely to be in different geographical groups compared to the methods that consider energy. Thus, it is expectable that these neighbouring buildings that would optimally take the same decision will be treated differently.

Selecting concrete solutions that are comparable between the four clustering methods is not trivial. In particular, the Pareto-front will always be sampled with a limited resolution. This includes that particular weightings of optimisation goals, especially extreme weightings like the cheapest solution, might not be sampled – as mentioned before.

First we select the solution with the lowest possible investment that still has energy costs in 2025 that are below 500 €/Pers. In Fig. 10, this region looks densely sampled with a similarly shaped Pareto plane. The filtered solutions are listed in Tab. 3. By design, all four configurations match the desired energy

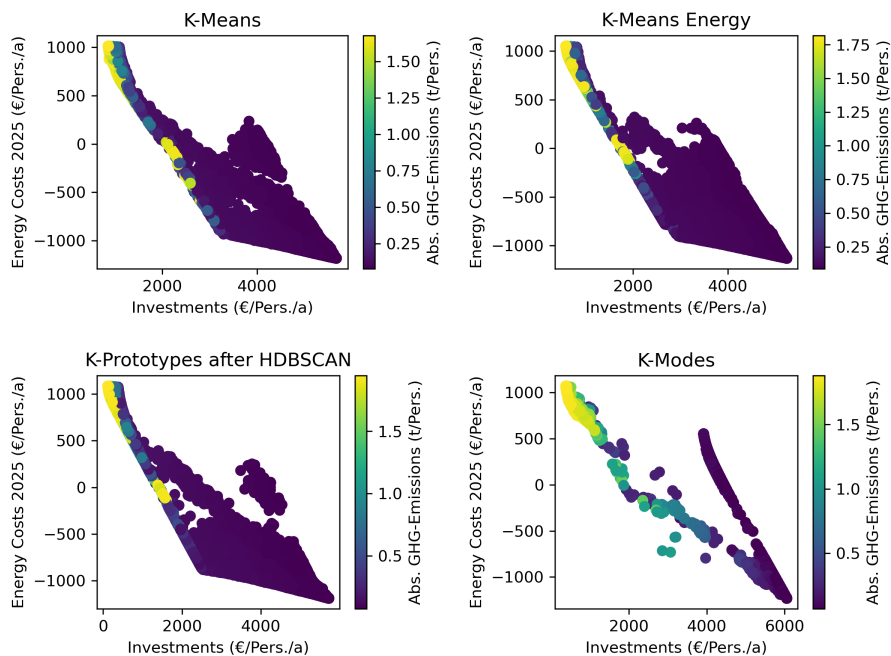


Figure 10: Pareto-plane in the space of conflicting goals. Starting from the low-investment edge, investment can first reduce both, operational costs and emissions. However, assuming energy costs of 2025, investments need to be subsidised to be profitable.

costs. The lowest possible investment, however, deviates in a range between 756 €/Pers/a and 1339 €/Pers/a. For the emissions, two of the solutions show values of approximately 1.2t/Pers and two of approximately 1.7t/Pers. In total, the solution found by K-Means Energy can be considered the best, K-Prototypes is better than K-Means (without energy information), but there is no strictly worst solution. As we searched for low investment costs, gas boilers have the biggest share of all heating technologies. The share goes from 87.8% (K-Means) down to 57.6% (K-Modes). All but K-Means (not heat-pumps at all) prefer heat-pump over heat-network. The choice per building is visualised in Fig. 11. The three of the algorithms that place decentralised heat pumps, show a high overlap (183 buildings assigned consistently). Assignment of heat network, however, is very inconsistent with only two buildings being attached to the heat network in three out of four cases.

Second, we select the configuration with a minimum of 33% of buildings using both, heat network and heat pump, that has the lowest investment annuity. We chose this specific configuration to find out which areas and buildings prefer which technology in a more or less equally distributed system. The filtered results are summarized in Tab. 4. It can be seen that the configurations

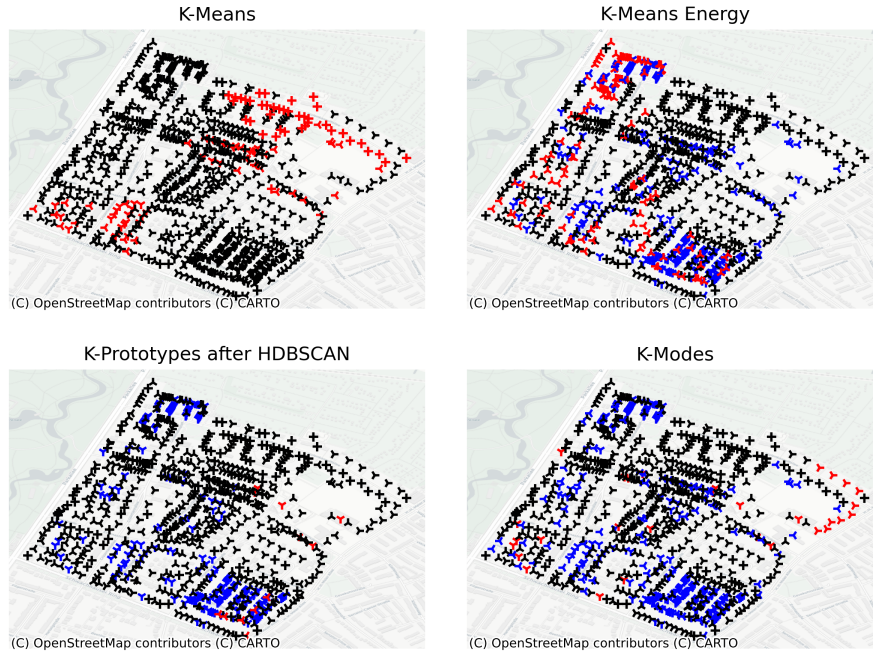


Figure 11: Technology choice in selected solutions based on grouping method (see Tab.3). Heat network (red), heat pump (blue), gas boiler (black).

show similar investment costs (2572 €/Pers/a to 2924 €/Pers/a) and emissions (0.11 t/Pers to 0.22 t/Pers), but deviate in the energy costs in 2025 with values ranging from a revenue of 339 €/Pers to spendings of 138 €/Pers. Interestingly, there is a tendency that the solutions with slightly lower investment costs tend to prefer lower penetration with gas boilers. Still, the filter makes sure that all three technologies are used in a significant number of buildings, as also seen in Fig. 12.

When comparing the three maps, it can be seen that some of the buildings show a clear preference over all four methods, while others are assigned different technologies between the runs. This is independent from the assigned archetype building. A numeric evaluation yields that 10.4% of the buildings are consistently assigned a gas boiler, 6.4% a heat pump, and 5.6% a heat network connection across all three of the favoured methods. While it sounds underwhelming that only less than a third of the buildings have the heating technology chosen independent from the grouping method, the numbers are still significantly bigger compared to purely random assignment (5.0%, 3.4%, and 2.4%, respectively).

The sensitivity of the result on the used clustering method can be interpreted in two different ways: It is possible that the clustering can introduce a considerable error, but it is also possible that the selected region for the study is

Quantity	Unit	K-Means	K-Means Energy	K-Prototypes after HDBSCAN	K-Modes
Heat Network	bldg	105	115	12	30
Heat Pump	bldg	0	249	197	258
Gas Boiler	bldg	754	495	650	571
Investments	€/Pers/a	1339	756	1211	1133
Energy Costs 2025	€/Pers	499	497	499	500
Emissions	t/Pers	1.64	1.17	1.16	1.70

Table 3: Configurations with lowest investment costs that have a limit of 500 €/Pers of energy costs in 2025. Best and close to best values are bold.

Quantity	Unit	K-Means	K-Means Energy	K-Prototypes after HDBSCAN	K-Modes
Heat Network	bldg	285	290	348	311
Heat Pump	bldg	269	289	199	372
Gas Boiler	bldg	305	280	312	176
Investments	€/Pers/a	2924	2642	2572	2783
Energy Costs 2025	€/Pers	-86	-339	-412	138
Emissions	t/Pers	0.11	0.12	0.12	0.22

Table 4: Configurations with lowest investment that have at least 33% of both, heat network and heat pump. Best and close to best values are bold.

so homogenous that even small inaccuracies change the result significantly. In the latter case, the deviation between the results would imply that the choices do not make a big difference. The overall shape of the Pareto-space as depicted in Fig. 10 supports this interpretation at least for three of the investigated methods.

6 Conclusion

This study presented a method to preprocess and aggregate geodata to be able to optimise the energy system configuration of an ensemble of a large number of buildings. After the selection of the area, all presented steps can in be applied in an automatic workflow without any manual input. While details of the actual results depend on simulation parameters, the overall performance of investigated clustering methods is comparable. In our study, methods that balance influence of geographic location and energy properties (K-Means Energy and K-Prototypes after HDBSCAN) showed the best performance. In particular, not considering energy at all when building geographical groups hides options for very small heating grids just between similar buildings in close proximity. While the low number of variables was a disadvantage here, it should be noted that K-Modes might still be advantageous if a more complex energy system model was used. Especially when including more representative buildings, storage and

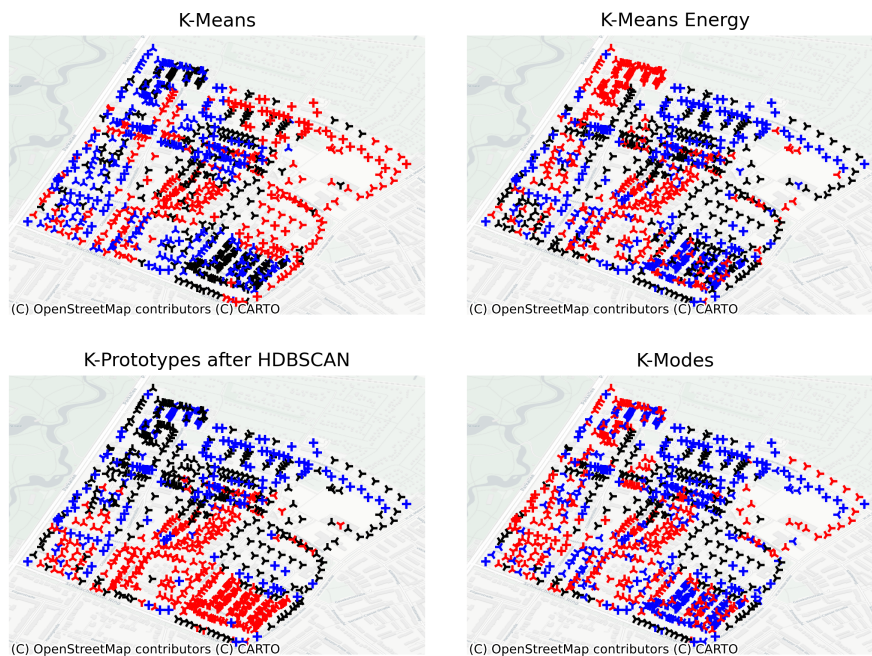


Figure 12: Technology choice in selected solution based on grouping method (see Tab.4). Heat network (red), heat pump (blue), gas boiler (black).

optimised energy-exchange between the buildings, the overall runtime might increase to an extent, that the expected advantage in run-time might outweigh the reduced number of options.

We made the choice to use building parameters normalised by the building footprint to allow for a low number of representative buildings all representing a similar number of real buildings. In particular, we also normalised the costs of a connection to a heating grid. The alternative choice of non-normalised buildings would allow for non-linear investment costs. If the model still stays in a linearisable regime, even the argument about commutable operation from the introduction stays applicable. However, better representation with lower number of representatives seems to be more important at the moment. Note that this argument might be invalidated if other highly non-linear investment options come into scope, resulting in a higher number of variables for the normalised representation.

For future work, we suggest to test the method including the different grouping methods with another region to assess whether an area with clear advantages of one technology is correctly identified. This might be at the edge of a town where a densely populated area transitions into a more rural area. Also, the method to use representative roofs should be validated and possibly fine-tuned. Lastly, it would be interesting to include additional demands and technologies,

esp. cooling demand and bidirectional heat networks.

Declarations

Acknowledgements

The authors thank “wesernetz” for the provision of the real-world heat demand data used in the use case scenario. They also acknowledge Diana Maldonado for contributing code for the Pareto-optimisation and for valuable discussions, in particular about the selection of representative configurations.

Author contributions

Patrik Schönfeldt: conceptualization, methodology, software, formal analysis, investigation, writing – original draft; Elif Turhan: methodology, writing – reviewing and editing.

Funding

This work has been funded by the German Federal Ministry of Research, Technology and Space as part of the Project “Wärmewende Nordwest”, Grant No. 03SF0624L.

Data availability

The current study uses heat data received under a no-disclosure agreement. Conditions apply to access the data.

Appendix A Two-step clustering scan

As described in Sec. 3, we implemented a two-step clustering method, where a data-driven definition of representative buildings is followed by a geographical grouping of these. Details on the applied grouping methods can be found in 3.2.

Here, we present the result of a scan over the number of both, representative buildings and geographical groups, show how these effect the number of variables needed to describe the final model and the average single-group line length, which we take as a measure for geographical cohesion of the grouping method. The results are visualised in Fig. 13. In the figure, the right hand side shows the average length of a heat network, if heat networks were built connecting all buildings in the same geographical group. The left hand side displays the number of existing combinations between building category and geographical group. This translates to the number of variables needed in an optimisation model.

Depending on the method used for geographical grouping, increasing the number of these groups does not decrease the geographical cohesion. For both

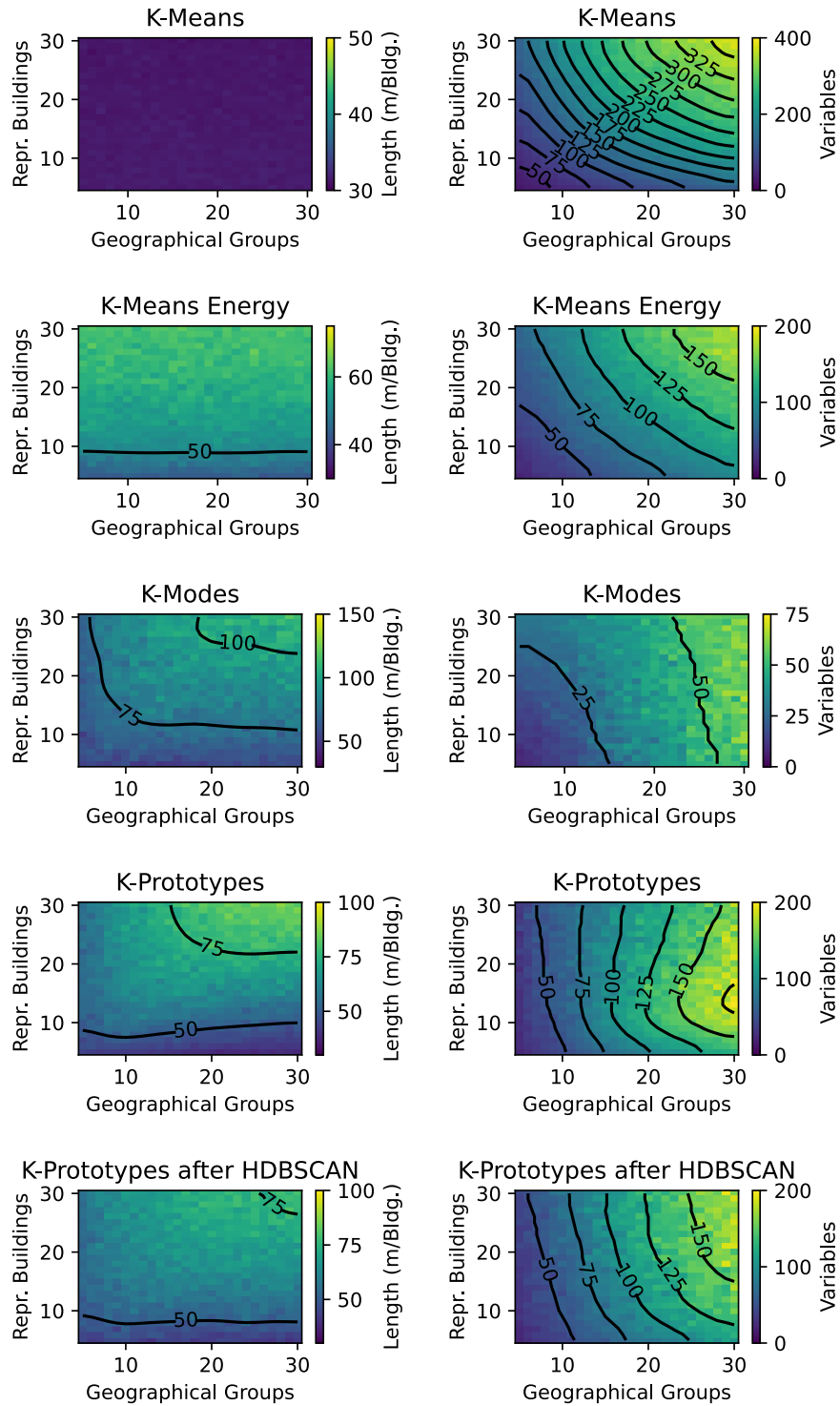


Figure 13: Average single-group line length (left) and number of variables (right). We introduced smoothed lines to guide the eye. Note that these are not 100% accurate.

K-Prototypes approaches and K-Modes this is no longer true if the number of representative buildings is increased too much for the targeted number of geographical groups. The absolute number of variables is clearly highest for purely geographical K-Means. This is no surprise as it has no mechanism to group similar buildings. K-Means including energy as well as both approaches using K-Prototypes show similar performance in this indicator, with an advantage of K-Prototypes when the number of representative buildings is increased for a constant number of geographical groups. By favourably grouping the same representative buildings in one geographical group, K-Modes manages to keep the number of variables lowest. For K-Prototypes without HDBSCAN, we observe that increasing the number of representative buildings for high number of geographical groups can decrease the number of variables. As the total number of variables is still relatively high, we did not investigate this effect further.

Appendix B Energy system model

For the present study, we apply an energy balance model without any storage. The time series for heat demand, PV potential, and the COP curve of the air source heat pump are calculated from the typical meteorological year for the area (TMY of 2015, tile 530876088493) as published by the DWD (Deutscher Wetterdienst, German Weather Service) [29]. Using this weather time series, annual energy demand is converted to energy time series using the software `demandlib` [15]. We also use the air temperature of the TMY as the source temperature $T_S(t)$ to calculate the efficiency of the decentralised air source heat pumps as

$$1/\eta_C(t) = c_{\text{pf}} \times \frac{T_F}{T_F - T_S(t)} \quad (8)$$

assuming a constant thermodynamic efficiency of $c_{\text{pf}} = 0.45$, and a global flow temperature of $T_F = 328.15$ K. The irradiation data can be used to calculate the solar power potential time series using `PVLib` [30] and Eq. (2) as

$$P_{\text{PV},b}(t) = \frac{A_b}{1 \text{ m}^2} \sum_{n=0}^{N-1} \omega_{n,b} \times P_n(t). \quad (9)$$

The building energy balance depends on the decision of the heating technology. We define $\delta_{\text{HP},b,g} = 1$ if representative building b in group g uses a heat pump, $\delta_{\text{GB},b,g} = 1$ for a present gas boiler, and $\delta_{\text{HN},b,g} = 1$ if the building is connected to the heat network. In our present model, the heat supply options are mutually exclusive, meaning

$$\delta_{\text{HP},b,g} + \delta_{\text{GB},b,g} + \delta_{\text{HN},b,g} = 1. \quad (10)$$

PV investment, on the other hand, is assumed to be continuous $0 \leq q_{\text{PV},b,g} \leq 1$. From this, the time series for the building energy balance can be calculated as

$$P_{\text{el},b,g}(t) = P_{\text{ESLP},b}(t) + \frac{\delta_{\text{HP},b,g}}{\eta_{C,b}(t)} P_{\text{HSLP},b}(t) - q_{\text{PV},b,g} P_{\text{PV},b}(t), \quad (11a)$$

for electricity and

$$P_{\text{gas},b,g}(t) = \delta_{\text{GB},b,g} \times P_{\text{HSLP},b}(t) \quad (11b)$$

for gas. The remaining power time series for the central heat pump is

$$P_{\text{el},\text{HN}}(t) = \frac{1}{\eta_{\text{C},b}(t)} \sum_{b \in \mathfrak{B}} \sum_{g \in \mathfrak{G}} \delta_{\text{HN},b,g} P_{\text{HSLP},b}. \quad (11c)$$

Further, for the emissions as defined in Eq. (7c), the global energy balance is relevant. We have

$$P_{\text{el}}(t) = \sum_{b \in \mathfrak{B}} \sum_{g \in \mathfrak{G}} P_{\text{el},b,g}(t) + P_{\text{el},\text{HN}}(t) \quad (12a)$$

for electricity, and

$$P_{\text{gas}}(t) = \sum_{b \in \mathfrak{B}} \sum_{g \in \mathfrak{G}} P_{\text{gas},b,g}(t) \quad (12b)$$

for gas.

Using the corresponding power time series, the energy costs in 2025 of representative building b in group g as used in Eq. (7a) is

$$\begin{aligned} C_{b,g} = & c_{\text{el}} \int \max(P_{\text{el},b,g}(t), 0 \text{ kW}) \, dt \\ & - c_{\text{feedin}} \left| \int \min(P_{\text{el},b,g}(t), 0 \text{ kW}) \, dt \right| \\ & + c_{\text{gas}} \int P_{\text{gas},b,g}(t) \, dt. \end{aligned} \quad (13a)$$

The respective costs are $c_{\text{el}} = 0.3 \text{ €/kWh}$, $c_{\text{feedin}} = 0.08 \text{ €/kWh}$, and $c_{\text{gas}} = 0.1 \text{ €/kWh}$. The energy costs for the heat network $C_{\text{el},\text{HN}}$ are assumed to be proportional to its energy demand

$$C_{\text{el},\text{HN}} = c_{\text{el}} \int P_{\text{el},\text{HN}}(t) \, dt. \quad (13b)$$

Assuming the same electricity costs for households and the heat network operator is a simplification made to make the results easier to understand focussing on the differences due to the aggregation. It also compensates for the optimistically high COP when it comes to the cost calculation.

Considering the investment cost, to allow for more flexibility when deciding about algorithms for the heuristic Pareto-optimisation, investment decision is not taken to be discrete. Instead, we introduce $0 \leq q_{\text{HP},b,g} \leq 1$, and $0 \leq q_{\text{HN},b,g} \leq 1$ as continuous decision variables. They are rounded to obtain the energy system model values

$$\delta_{h,b,g} = \lfloor q_{h,b,g} + 0.5 \rfloor \quad (14a)$$

for $h \in \{\text{HP}, \text{HN}\}$. For the actual investment, we then use the upper limit of the two

$$\hat{q}_{h,b,g} = \max(q_{h,b,g}, \delta_{h,b,g}), \quad (14b)$$

so that there is an incentive for the heuristic to converge to single-technology solutions. Finally, to compute the investment as defined in Eq. (7b), we apply price scaling curves using values of [16]. The costs of building heat pumps then are

$$C_{\text{HP},b,g} = \hat{q}_{\text{HP},b,g} \times \frac{\hat{P}_{\text{heat}}^{0.705}}{1 \text{ kW}} \times \frac{3830.5 \text{ €}}{20 \text{ a}}. \quad (15a)$$

For peak powers $\hat{P}_{\text{heat}} \geq 50 \text{ kW}$, specifically for the heat network, the constants are first changed to 0.793 and 3194.6 €, and from 300 kW on to 0.755 and 1352.0 €. For PV systems we assume

$$C_{\text{PV},b,g} = P_{\text{PV},b,g} \times \frac{1500 \text{ €/kW}}{20 \text{ a}}. \quad (15b)$$

The costs of the connection of a building to the heat network are

$$C_{\text{HN},b,g} = \frac{\hat{q}_{\text{HN},b,g}}{25 \text{ a}} \times \left(\frac{\hat{P}_{\text{heat}}}{1 \text{ kW}} \times 13.4 \text{ €} + 13976 \text{ €} \right). \quad (15c)$$

Finally, the contribution of the heat network infrastructure itself is

$$C_{\text{HN}} = l_{\text{HN}} \times \frac{\hat{P}_{\text{heat}}^{0.2029}}{1 \text{ kW}} \times \frac{432.69 \text{ €}}{50 \text{ a}} + C_{\text{HP}}, \quad (15d)$$

with the length of the heat network l_{HN} and the cost of the central heat pump C_{HP} calculated according to Eq. (15a). As mentioned earlier, we assumed gas boilers to be existing and thus set $C_{\text{GB}} = 0 \text{ €/a}$. This is despite the fact that replacements might be needed, and mainly to have a known Pareto-optimal solution for testing the aggregation methods.

References

- [1] Turkey IEA. Energy policy review. *International Energy Agency*, 2020.
- [2] Andrea Arnold-Drmic. Wärmewende in Deutschland: Status quo der Kommunalen Wärmeplanung. *BBSR-Analysen KOMPAKT*, 7:2024, 2024.
- [3] Donald Goldfarb. *On the Complexity of the Simplex Method*, pages 25–38. Springer Netherlands, Dordrecht, 1994.
- [4] Ana Rita Amaral, Eugénio Rodrigues, Adélio Rodrigues Gaspar, and Álvaro Gomes. Review on performance aspects of nearly zero-energy districts. *Sustainable Cities and Society*, 43:406–420, 2018.

- [5] Luis Blanco, Alaa Alhamwi, Björn Schiricke, and Bernhard Hoffschmidt. Data-driven classification of urban energy units for district-level heating and electricity demand analysis. *Sustainable Cities and Society*, 101:105075, 2024.
- [6] Marta Gangoells, Miquel Casals, Núria Forcada, Marcel Macarulla, and Eva Cuerva. Energy mapping of existing building stock in Spain. *Journal of Cleaner Production*, 112:3895–3904, 2016.
- [7] Tobias Loga, Britta Stein, and Nikolaus Diefenbach. Tabula building typologies in 20 European countries—making energy-related features of residential building stocks comparable. *Energy and Buildings*, 132:4–12, 2016. Towards an energy efficient European housing stock: monitoring, mapping and modelling retrofitting processes.
- [8] Giuliano Dall’O’, Annalisa Galante, and Marco Torri. A methodology for the energy performance classification of residential building stock on an urban scale. *Energy and Buildings*, 48:211–219, 2012.
- [9] Brian Cody, Wolfgang Loesch, and Alexander Eberl. Operating energy demand of various residential building typologies in different European climates. *Smart and Sustainable Built Environment*, 7(3-4):226–250, 09 2018.
- [10] Simone Giostra, Gabriele Masera, and Rafaella Monteiro. Solar typologies: A comparative analysis of urban form and solar potential. *Sustainability*, 14(15), 2022.
- [11] Narjes Abbasabadi and Mehdi Ashayeri. Urban energy use modeling methods and tools: A review and an outlook. *Building and Environment*, 161:106270, 2019.
- [12] Jouri Kanters, Maria Wall, and Elisabeth Kjellsson. The solar map as a knowledge base for solar energy use. *Energy Procedia*, 48:1597–1606, 2014. Proceedings of the 2nd International Conference on Solar Heating and Cooling for Buildings and Industry (SHC 2013).
- [13] Bundesamt für Kartographie und Geodäsie. 3d building models lod2 Germany (lod2-de). <http://data.europa.eu/88u/dataset/31bedca5-1843-4254-a168-1acda618c0b4>, 2024.
- [14] Parth Umeshbhai Vachhani. Influence of spatial clustering on the result of heat supply system optimization. Master’s thesis, Hochschule Nordhausen, 2025.
- [15] Uwe Krien, Patrik Schönfeldt, Birgit Schachler, Joris Zimmermann, Jann Launer, Francesco Witte, Florian Maurer, Amedeo Ceruti, Caroline Möller, Marie-Claire Gering, gplssm, Gregor Becker, Sascha Birk, Stephen Bosch, and henhuy. oemof/demandlib: v0.2.2, 04 2025.

- [16] Nora Langreder, Frederik Lettow, Malek Sahnoun, Sven Kreidelmeyer, Aurel Wunsch, and Saskia Lengning. Technikkatalog Wärmeplanung. Technical report, ifeu – Institut für Energie- und Umweltforschung Heidelberg, Öko-Institut e.V., IER Stuttgart, adelphi consult GmbH, Becker Büttner Held PartGmbH, Prognos AG, 2024.
- [17] F. Pedregosa, G. Varoquaux, A. Gramfort, V. Michel, B. Thirion, O. Grisel, M. Blondel, P. Prettenhofer, R. Weiss, V. Dubourg, J. Vanderplas, A. Passos, D. Cournapeau, M. Brucher, M. Perrot, and E. Duchesnay. Scikit-learn: Machine learning in Python. *Journal of Machine Learning Research*, 12:2825–2830, 2011.
- [18] Erich Schubert and Lars Lenssen. Fast k-medoids clustering in rust and python. *Journal of Open Source Software*, 7(75):4183, 2022.
- [19] Martin Ester, Hans-Peter Kriegel, Jörg Sander, and Xiaowei Xu. A density-based algorithm for discovering clusters in large spatial databases with noise. In *Proceedings of the Second International Conference on Knowledge Discovery and Data Mining*, KDD’96, page 226–231. AAAI Press, 1996.
- [20] Mihael Ankerst, Markus M. Breunig, Hans-Peter Kriegel, and Jörg Sander. Optics: ordering points to identify the clustering structure. In *Proceedings of the 1999 ACM SIGMOD International Conference on Management of Data*, SIGMOD ’99, page 49–60, New York, NY, USA, 1999. Association for Computing Machinery.
- [21] Ricardo J. G. B. Campello, Davoud Moulavi, and Joerg Sander. Density-based clustering based on hierarchical density estimates. In Jian Pei, Vincent S. Tseng, Longbing Cao, Hiroshi Motoda, and Guandong Xu, editors, *Advances in Knowledge Discovery and Data Mining*, pages 160–172, Berlin, Heidelberg, 2013. Springer Berlin Heidelberg.
- [22] ZHEXUE HUANG. Extensions to the k-means algorithm for clustering large data sets with categorical values. *Data Mining and Knowledge Discovery*, 2:283–304, 1998.
- [23] Nelis J. de Vos. kmodes categorical clustering library. <https://github.com/nicodv/kmodes>, 2015–2021.
- [24] R.L. Graham and Pavol Hell. On the history of the minimum spanning tree problem. *Annals of the History of Computing*, 7(1):43–57, 1985.
- [25] Walter Winter, Thomas Haslauer, and Ingwald Obernberger. Untersuchungen der Geichzeitigkeit in kleinen und mittleren Nahwärmenetzen. *Euroheat & Power*, 2001.
- [26] Lucas Schmeling, Patrik Schönfeldt, Peter Klement, Lena Vorspel, Benedikt Hanke, Karsten von Maydell, and Carsten Agert. A generalised optimal design methodology for distributed energy systems. *Renewable Energy*, 200:1223–1239, 2022.

- [27] K. Deb, A. Pratap, S. Agarwal, and T. Meyarivan. A fast and elitist multiobjective genetic algorithm: Nsga-ii. *IEEE Transactions on Evolutionary Computation*, 6(2):182–197, 2002.
- [28] Francesco Biscani and Dario Izzo. A parallel global multiobjective framework for optimization: pagmo. *Journal of Open Source Software*, 5(53):2338, 2020.
- [29] <https://www.dwd.de/DE/leistungen/testreferenzjahre/testreferenzjahre.html>.
- [30] Kevin S. Anderson, Clifford W. Hansen, William F. Holmgren, Adam R. Jensen, Mark A. Mikofski, and Anton Driesse. pvlb python: 2023 project update. *Journal of Open Source Software*, 8(92):5994, 2023.